Superlattices and Microstructures 80 (2015) 80–90

Contents lists available at ScienceDirect

Superlattices and Microstructures

journal homepage: www.elsevier.com/locate/superlattices

Mechanical stabilities and nonlinear properties of monolayer Gallium sulfide under tension

Chuanghua Yang [a,*], Pengfei Lu [b], Wendeng Huang [a], Jun Chen [c]

[a] School of Physics and Telecommunication Engineering, Shaanxi University of Technology (SNUT), Hanzhong 723001, Shaanxi, China
[b] State Key Laboratory of Information Photonics and Optical Communications, Beijing University of Posts and Telecommunications (BUPT), P.O. Box 72, Beijing 100876, China
[c] Beijing Applied Physics and Computational Mathematics, Beijing 100088, China

ARTICLE INFO

Article history:
Received 28 September 2014
Accepted 2 October 2014
Available online 22 October 2014

Keywords:
Monolayer GaS
Nonlinear elastic response
Ultimate stress
Ultimate strain
First-principles

ABSTRACT

The mechanical stabilities and nonlinear properties of monolayer Gallium sulfide (GaS) under tension are investigated using density functional theory (DFT). The ultimate stresses and ultimate strains, and the structure evolutions of monolayer GaS under armchair, zigzag, and equiaxial tensions are predicted. A thermodynamically rigorous continuum description of nonlinear elastic response is given by expanding the elastic strain energy density in a Taylor series in Lagrangian strain truncated after the fifth order term. Fourteen nonzero independent elastic constants are determined by least-square fit to the DFT calculations. Pressure dependent elastic constants ($C_{ij}(P)$) and pressure derivatives of $C_{ij}(P)$ (C'_{ij}) are also calculated. Calculated values of ultimate stresses and strains, and the in-plain Young's modulus are all positive. It proves that monolayer GaS is mechanically stable.

1. Introduction

Graphene is a two-dimension (2D) honeycomb monolayer of carbon atoms, known as the strongest 2D material ever measured by experiments [1]. In the past ten years, graphene has always been a research hot spot in the field of material science due to its unique physical, chemical and mechanical

* Corresponding author.
E-mail address: chuanghua888@gmail.com (C. Yang).

http://dx.doi.org/10.1016/j.spmi.2014.10.019
0749-6036/

properties. These non-trivial properties of graphene make it possess great research value and lots of promising applications in numerous fields, such as semiconductor devices and biomedical [2].

Although graphene possesses high electron and hole mobility, its zero bandgap energy hinders their applications in microelectronics and optoelectronics [3,4]. In order to overcome these limits, the explorations of other graphene-like 2D atomic-layer crystals have been reported including isolated mono- and few-layers of hexagonal boron nitride (*h*-BN) [5,6], transition metal dichalcogenides (TMDs, e.g., MoS_2 [6–11], WS_2 [12,13], and WSe_2 [14,15]), and metal monochalcogenides (e.g., GaSe [16–19], GaS [19,20], and InSe [21]). Most of materials are semiconductors and are naturally abundant, which can be used for building the next-generation electronic and optoelectronic devices.

Although most researches have focused on 2D TMDs, recently 2D layered metal monochalcogenides have also attracted increasing interest [16–21]. Recent studies on these 2D metal monochalcogenides demonstrate that they have significantly different electronic and optoelectronic properties from the TMDs. Gallium sulfide (GaS) is a typical layered metal monochalcogenides, which has an indirect bandgap energy of 2.59 eV and a direct bandgap energy of 3.05 eV [22]. GaS is composed of covalently bonded S–Ga–Ga–S atoms, with a lattice constants 3.59 Å and D_{3h} symmetry [23]. Single-layer or few-layer GaS nanosheets have been fabricated using a mechanical cleavage approach and successfully been transferred to SiO_2/Si wafer and other substrates [24]. 1D GaS nanowires and nanobelts have also been synthesized using a vapor–solid method and exhibited strong photoluminescence and field-emission behavior [25,26]. Ultrathin GaS bottom-gate transistors with mobilities of 0.1 $cm^2\,V^{-1}\,s^{-1}$ have been achieved by Dravid et al. [19]. Recently, Pingan Hu and his co-workers have fabricated highly responsive photodetectors consisting of GaS nanosheets on both rigid (SiO_2/Si) and flexible (polyethylene terephthalate) substrates [20]. They have also demonstrated that 2D GaS nanosheets photodetectors is superior to those of bulk GaS, pristine graphene, and InGaAs. In a word, 2D GaS has highly potential in building microelectronic and optoelectronic devices.

The mechanical properties are crucial for designing and manufacturing devices with 2D nanomaterials in practice. Strain engineering is also a common and effective approach to tailor the electronic properties of materials and the performance of the devices. In addition, it is available to apply equiaxial or uniaxial strain to 2D materials through the substrates. Therefore, it is important and significant to understand the mechanical properties of monolayer GaSe for tuning its electronic properties by strain engineering. The mechanical properties (nonlinear elastic properties, ultimate strength and so on) of the typical 2D materials: graphene [27,28], silicene [29], MoS_2 [11], have been studied extensively. However, so far, the mechanical properties of monolayer GaS have been investigated rarely and especially its nonlinear high-order elastic responses have not been reported.

The overall objective of this work is to investigate the ultimate strength, stabilities and nonlinear elasticity of monolayer GaS. We first use the DFT to calculate the response of GaS along equiaxial (EQ) tension and uniaxial tensions along zigzag (ZZ) and armchair (AC) directions to obtain the ultimate strengths and ultimate strains for these deformations. The magnitude of the applied tensions ranges from infinitesimal to finite deformations beyond that corresponding to the intrinsic (i.e., maximum) stress. We perform a series of from first-principles calculations to get the strain energy density and stress tensors of monolayer GaS under three types of tensions along AC, ZZ, and EQ directions. Nonlinear elastic response is established by expanding strain energy density in a Taylor series with respect to Lagrangian strain. The independent high-order constants are determined by fitting the continuum model to the 2nd P–K stress versus Lagrangian strain relationships by DFT calculations. Our results of continuum formulation could be useful in finite element modeling of the mechanical properties of monolayer GaS.

2. Density functional calculations

The total energies of the systems, forces on each atom, stresses, and stress–strain relationships of monolayer GaS under the desired deformation configurations are characterized via DFT calculations. DFT calculations are carried out with the Vienna Ab initio Simulation Package (VASP) [30,31], which is based on the DFT. The electrons explicitly included in the calculations are the $4s^24p^1$, and $3s^23p^4$ electrons for Ga and S atoms, respectively. The core electrons was replaced by the projector

augmented-wave (PAW) [32,33] and pseudo-potential approach. The exchange–correlation potentials is approximated by local-density approximation (LDA) [32].

For all studies here, the height of out-of-plane axis in unite cell is maintained at 16 Å to eliminate the interactions. The k-point mesh densities for (2×1) unit cell correspond to $36 \times 18 \times 1$ Gamma centered grid. The kinetic-energy cutoff of the plane wave for all calculation is set at 600 eV. In the optimization process, a total energy convergence criterion of 1.0×10^{-6} eV per atom is applied. In order to relax as much as possible watching the residual forces, the max convergence threshold for the maximum force is specified as -1.0×10^{-5} eV/Å per atom. The calculations are performed at zero temperature.

Fig. 1 shows the monolayer GaS atomic unit cell under three types of tension: AC uniaxial tension (Fig. 1a), ZZ uniaxial tension (Fig. 1c), undeformed or EQ tension (Fig. 1b). We first optimize the equilibrium geometric structure of monolayer GaS. The equilibrium lattice a_0 is 3.53 Å, which is very approximation to the lattice constant of bulk GaS 3.59 Å. The length of Ga–S bond $d_1 = d_2$ is 2.308 Å and the length of Ga–Ga bond d_3 is 2.409 Å. The strain energy density versus strain and stress–strain relationships calculations for both AC and ZZ uniaxial tensions are performed through the (2×1) unit cell in Fig. 1b. We will state the implement of uniaxial tension through the example of 0.01 AC uniaxial tension: the lattice constant along AC direction is fixed at $1.01a_0$ and the lattice constant along ZZ direction remain unchanged (e.g., the strain is 0). Then relax the system to minimum energy. Calculated geometric structures of deformed monolayer GaS show that there exist additional internal relative displacements beyond the affine displacements under uniaxial tension. The EQ tension is imposed by uniformly pulling the primitive cell. The DFT calculations validate there is no internal relative displacement within the primitive cells when GaS undergoes EQ tension. This is consistent with the graphene's results in previous studies [27,33].

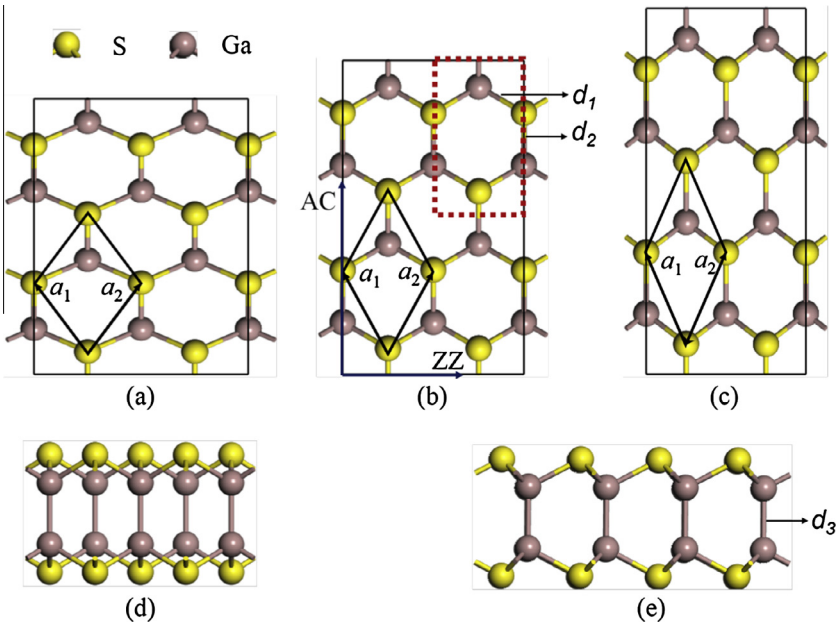

Fig. 1. Atomic structure of monolayer GaS. (a) top view of uniaxially tensile in zigzag direction; (b) top view of undeformed or equiaxially tensile monolayer GaS; (c) top view of uniaxially tensile GaS along armchair direction; (d) (1 0 0) cross section side view of monolayer GaS; (e) (0 1 0) cross section side view of monolayer GaS. The yellow and purple spheres represent S and Ga atoms, respectively. The axes labeled by the blue arrows denote the armchair (AC) and zigzag (ZZ) directions, respectively. The (2×1) unit cell framed by red dots line in panel (b) is used to exert the uniaxial tensions along AC and ZZ directions (For interpretation of the references to colour in this figure legend, the reader is referred to the web version of this article.).

The VASP simulation calculates the Cauchy stress. For 2D monolayer GaS it must be expressed as a 2D Cauchy stress with units of N/m by multiplying the Cauchy stress with units of N/m^2 and the supercell thickness of 16 Å. The Cauchy stress is related to the 2nd Piola–Kirchhoff (P–K) stress Σ as

$$\sum = j\boldsymbol{F}^{-1}\boldsymbol{\sigma}(\boldsymbol{F}^{-1}), \tag{1}$$

where j is the determinant of the deformation gradient tensor $\boldsymbol{F}$.

3. Results and discusses

3.1. Atomic structure

In our study, the most energetically favorable structure is set as the strain-free structure. All the atoms are allowed full freedom of motion under the three types of tensions. The evolutions of atomic structures of monolayer GaS under the AC, ZZ, and EQ tensions are shown in the Fig. 2. The bond d_1 and d_2, are indicated in the Fig. 1b. When the AC tension is applied, the bond d_2 of monolayer GaS is parallel to the stretching force. And the bond length of d_2 monotonically increases with the strain, as illustrated in Fig. 2a. The variation of d_1 bond length with the AC strain is non-monotonic and is smaller relative to d_2. The d_1 bond length reaches its maximum value of 2.3385 Å at the strain of 0.150. When the ZZ tension is applied, the bond d_2 of monolayer GaS is perpendicular to the direction of tension and the change of its length is smaller relative to d_1. The bond length of d_1 monotonically increases with the strain. The length of bond d_2 non-monotonically varies with the ZZ tension and reaches its maximum value of 2.3152 Å at the strain of 0.095. When the EQ tension is applied on monolayer GaS, the lengths of bond d_1 and d_2 are equal and linearly increase with the increasing strain, as shown in Fig. 2c.

Bond d_3 is a Ga–Ga covalent bond between two Ga–S bonds, which is indicated in Fig. 1c. Fig. 3 shows the variation of bond d_3 in monolayer GaS with the three types of tensions. In the harmonic region, the curves for armchair and zigzag tensions are almost identical. The anisotropy becomes more and more obvious as the increasing strain. The EQ tension with respective to the other uniaxial tensions makes bond d_3 more quickly increase. There is an inflection point at corresponding ultimate strain in the curve of bond length versus EQ tension relationship. This just is an evidence that plastic deformation occurs in monolayer GaS under EQ tension.

3.2. Strain energy density and stress versus Lagrangian strain relationships

We define strain energy $\boldsymbol{E_s} = (\boldsymbol{E_{tot}} - \boldsymbol{E_0})$, where $\boldsymbol{E_{tot}}$ is the total energy of the strained system, $\boldsymbol{E_0}$ is the total energy of the strain-free system. The strain energy density has the functional form $\boldsymbol{\Phi = \Phi(\eta)}$ and is defined as $\boldsymbol{E_s/V}$, where $\boldsymbol{V}$ is the volume of the undeformed supercell. The $\boldsymbol{\Phi(\eta)}$ of monolayer GaSe as the functions of strain in AC, ZZ, and EQ tensions are shown in Fig. 4. The harmonic region where the $\boldsymbol{\Phi(\eta)}$ is a quadratic function of Lagrangian strain is between $0 < \boldsymbol{\eta} < 0.015$. The stresses, derivatives of the strain energy density, are linearly increasing with the increase of strains in the harmonic region. Fig. 5 shows five relationships of the 2nd Piola–Kirchhoff (P–K) stress versus Lagrangian strain under three types of tensions obtained from the DFT calculations. By comparing with stress–strain curves along armchair and zigzag directions, we find that both of curves are linear variation and almost identical in the harmonic region. The anharmonic region corresponds to the scope of $\boldsymbol{\eta} > 0.01$, where the linear stress–strain relationship is invalid and higher order terms are not negligible. The curves along the AC and ZZ directions are anisotropic in the anharmonic region. The ultimate strength is the maximum stress that a material can withstand when being stretched, and the corresponding strain is the ultimate strain. If the strain applied to a material is beyond its ultimate strain, it will be meta-stable and be easily destroyed by long wave-length perturbations, vacancy defects, and high temperature effects. The ultimate strengths of monolayer GaSe under AC, ZZ, and EQ tensions are 8.624 N/m, 10.466 N/m, and 8.838 N/m, respectively. Corresponding ultimate strains are 0.244, 0.473, and 0.275, respectively. For the monolayer GaS, both values of ultimate strength and strain along ZZ direction are maximum relative to others' tensions. In other word, it means that both the strength and toughness of monolayer GaS along the ZZ direction are largest. Interestingly, from the Fig. 5c we can

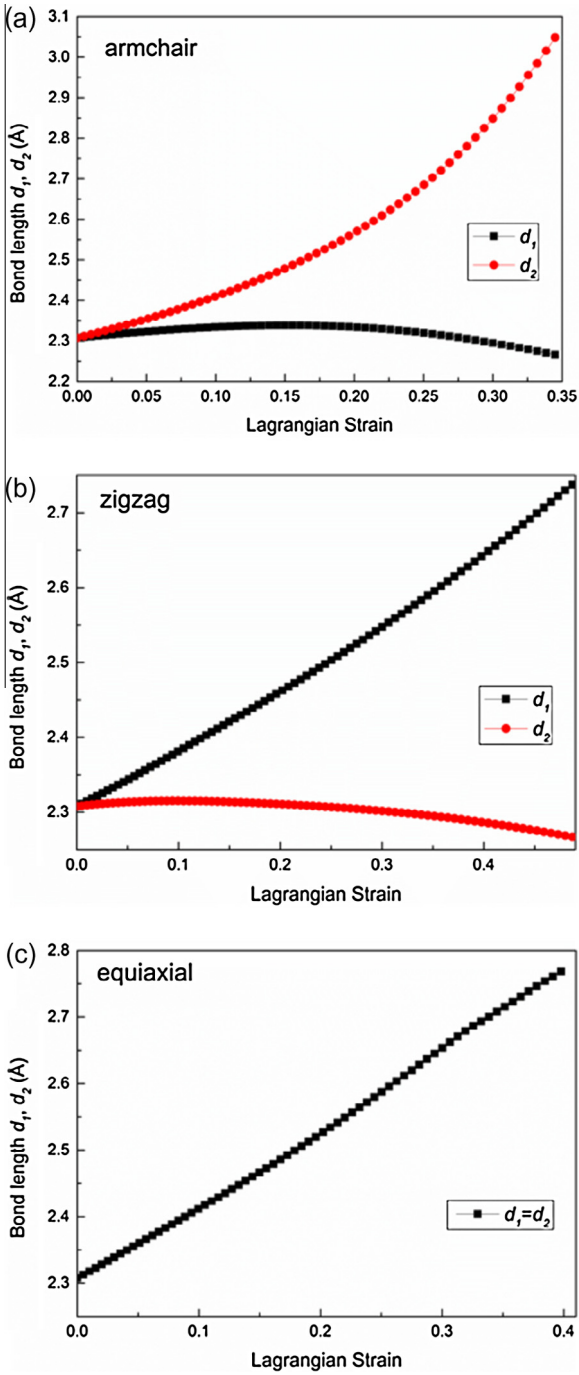

Fig. 2. Calculated dependences of bond d_1 and d_2 in monolayer GaS on (a) AC, (b) ZZ, and (c) EQ tensions. d_1 and d_2 are indicated in the Fig. 1b.

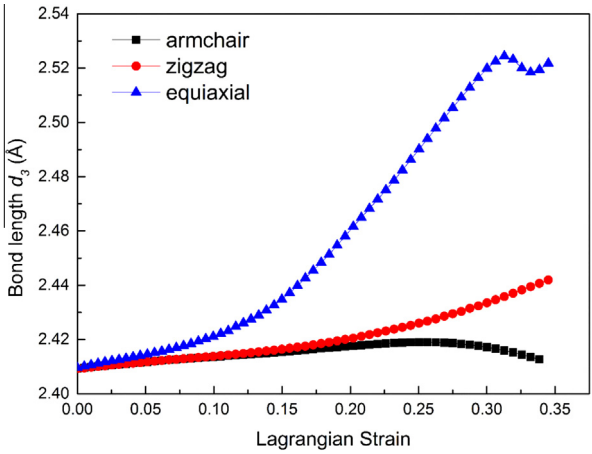

Fig. 3. Calculated dependence of bond d_3 in monolayer GaS on AC, ZZ, and EQ tensions. d_3 is indicated in the Fig. 1c.

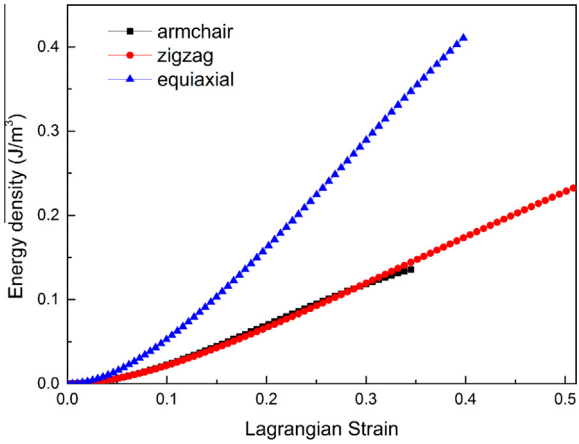

Fig. 4. Energy density versus strain relationships of monolayer GaS under AC, ZZ, and EQ tensions.

note that the discontinuity of curve appears at the ultimate strain. This means that monolayer GaS under EQ tension become mechanically stable and plastic deformation occurs. The above-mentioned study on atomic structure shows bond d_3 causes the plastic deformation of monolayer GaS.

3.3. The description of third-order nonlinear continuum elastic constants

The undeformed reference configuration is shown in Fig. 1b, with lattice vectors a_1 and a_2. When a macroscopically homogeneous deformation (deformation gradient tensor $\boldsymbol{F}$) applied, the lattice vectors of the deformed GaSe are $a_i' = \boldsymbol{F}a_i$ (with $i = 1,2$). The Lagrangian strain is defined as $\boldsymbol{\eta} = \frac{1}{2}(\boldsymbol{F}^T\boldsymbol{F} - \boldsymbol{I})$, where $\boldsymbol{I}$ is the identity tensor.

Nonlinear elastic constitutive behavior [34] is established by expanding $\boldsymbol{\Phi}$ in a Taylor series in terms of powers of Lagrangian strain $\boldsymbol{\eta}$ as

$$\boldsymbol{\Phi}(\boldsymbol{\eta}) = \frac{1}{2!}C_{ijkl}\eta_{ij}\eta_{kl} + \frac{1}{3!}C_{ijklmn}\eta_{ij}\eta_{kl}\eta_{mn} + \frac{1}{4!}C_{ijklmnop}\eta_{ij}\eta_{kl}\eta_{mn}\eta_{op} + \frac{1}{5!}C_{ijklmnopqr}\eta_{ij}\eta_{kl}\eta_{mn}\eta_{op}\eta_{qr} + \ldots, \tag{2}$$

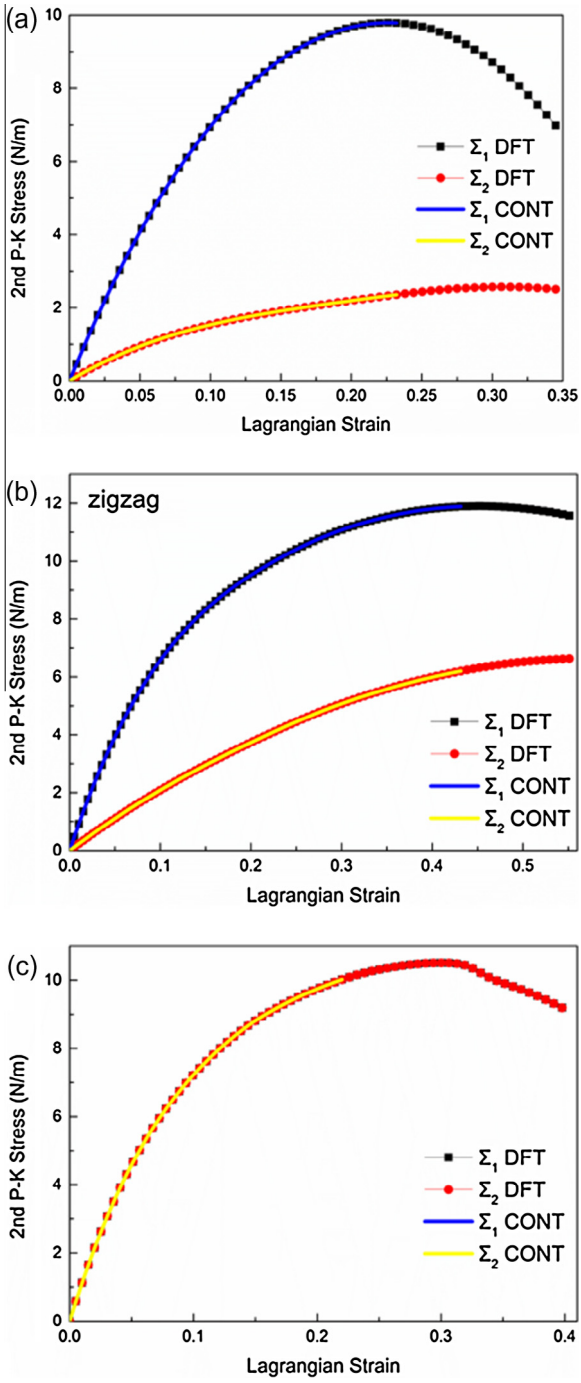

Fig. 5. Stress–strain responses of monolayer GaS under (a) AC, (b) ZZ, and (c) EQ tensions. Σ_1 (Σ_2) denotes the AC (ZZ) direction component of stress tensor.

where C_{ijkl}, C_{ijklmn}, $C_{ijklmnop}$, and $C_{ijklmnopqr}$ correspond to the second-order elastic constants (SOEC), third-order elastic constants (TOEC), fourth-order elastic constants (FOEC), and fifth-order elastic constants (FFOEC), respectively. The summation convention is adopted for repeating indices and summation for lower case indices runs from 1 to 3. The symmetric 2nd P–K stress tensor $\mathbf{\Sigma}_{ij}$ is

$$\Sigma_{ij} = \frac{\partial \mathbf{\Phi}}{\partial \eta_{ij}} = C_{ijkl}\eta_{kl} + \frac{1}{2!}C_{ijklmn}\eta_{kl}\eta_{mn} + \frac{1}{3!}C_{ijklmnop}\eta_{kl}\eta_{mn}\eta_{op} + \frac{1}{4!}C_{ijklmnopqr}\eta_{kl}\eta_{mn}\eta_{op}\eta_{qr} + \cdots \tag{3}$$

We use conventional Voigt notation [35] for subscripts: 11 → 1, 22 → 2, 33 → 3, 23 → 4, 31 → 5, and 12 → 6. Please note that for strain $\eta_4 = 2\eta_{23}$, $\eta_5 = 2\eta_{31}$, $\eta_6 = 2\eta_{12}$. The summation convention for upper case subscripts runs from 1 to 6. The Eq. (1) and Eq. (2) can be rewritten as:

$$\mathbf{\Phi} = \frac{1}{2!}C_{IJ}\eta_I\eta_J + \frac{1}{3!}C_{IJK}\eta_I\eta_J\eta_K + \frac{1}{4!}C_{IJKL}\eta_I\eta_J\eta_K\eta_L + \frac{1}{5!}C_{IJKLM}\eta_I\eta_J\eta_K\eta_L\eta_M + \cdots, \tag{4}$$

$$\Sigma_{ij} = \frac{\partial \mathbf{\Phi}}{\partial \eta_I} = C_{IJ}\eta_I + \frac{1}{2!}C_{IJK}\eta_I\eta_K + \frac{1}{3!}C_{IJKL}\eta_J\eta_K\eta_L + \frac{1}{4!}C_{IJKLM}\eta_J\eta_K\eta_L\eta_M + \cdots, \tag{5}$$

In this work, we assume that the contribution of bending to the strain energy density is negligible for all the tensions as compared to the in-plane strain contribution. This assumption is reasonable since the radius of curvature of out-of-plane deformation is significantly larger than the in-plane inter-atomic distance. Then we only consider the in-plane components for these kinds of structures.

The components of the SOEC, TOEC, FOEC, and FFOEC tensors can be simplified based on the symmetries of the graphene atomic lattice point group D_{6h}, which consists of a sixfold rotational axis and six mirror planes. Previous studies [11,27] have shown there are two, three, four, and five independent nonzero in-plane components for the SOEC, TOEC, FOEC, and FFOEC tensors, respectively.

The total fourteen independent elastic constants of monolayer GaSe are determined by a least-squares fitting to stress–strain relationships from DFT calculations. Five relationships between stress–strain are necessary and sufficient because there are five independent FFOECs. We obtain the relationships by simulating the following deformation states: uniaxial tensions in the AC and ZZ directions, and EQ tension. For uniaxial tension in the ZZ direction ($\eta_{ZZ} > 0$, $\eta_{AC} = 0$), the strain tensor is

$$\eta_{ij}^{ZZ} = \begin{pmatrix} 0 & 0 \\ 0 & \eta_{ZZ} \end{pmatrix}, \tag{6}$$

where η_{ZZ} is the amount of strain in ZZ direction.

For a given strain tensor, the associated deformation gradient tensor is not unique. The various possible solutions differ from one to another by a rigid rotation. Here the lack of a one-to-one map relationship between the strain tensor and deformation gradient tensor is not concern since the calculated energy is invariant under rigid deformation. One of the corresponding deformation gradient tensor $\boldsymbol{F}_{ZZ}$ for uniaxial strain in the ZZ direction is selected as

$$\boldsymbol{F}_{ZZ} = \begin{pmatrix} 1 & 0 \\ 0 & \varepsilon_{ZZ} + 1 \end{pmatrix}, \tag{7}$$

where ε_{ZZ} is the nominal strain along the ZZ direction. The 2nd P–K stress versus Lagrangian strain relationships for the uniaxial tension in the ZZ direction is

$$\Sigma_1^{zig} = C_{11}\eta_{ZZ} + \frac{1}{2}C_{111}\eta_{ZZ}^2 + \frac{1}{6}C_{1111}\eta_{ZZ}^3 + \frac{1}{24}C_{11111}\eta_{ZZ}^4, \tag{8}$$

$$\Sigma_2^{zig} = C_{12}\eta_{ZZ} + \frac{1}{2}C_{112}\eta_{ZZ}^2 + \frac{1}{6}C_{1112}\eta_{ZZ}^3 + \frac{1}{24}C_{11112}\eta_{ZZ}^4. \tag{9}$$

For uniaxial tension in the AC direction ($\eta_{AC} > 0, \eta_{ZZ} = 0$), the strain tensor is,

$$\eta_{ij}^{AC} = \begin{pmatrix} 0 & 0 \\ 0 & \eta_{AC} \end{pmatrix}, \tag{10}$$

One of the corresponding deformation gradient tensor $\boldsymbol{F}_{AC}$ for uniaxial tension in the AC direction is

$$\boldsymbol{F}_{AC} = \begin{pmatrix} 1 & 0 \\ 0 & \varepsilon_{AC} + 1 \end{pmatrix}, \tag{11}$$

where ε_{AC} is the nominal strain along the AC direction. The 2nd P–K stress versus Lagrangian strain relationships for AC tension are

$$\Sigma_1^{arm} = C_{12}\eta_{AC} + \frac{1}{2}(C_{111} - C_{222} + C_{112})\eta_{AC}^2 + \frac{1}{12}(C_{1111} + 2C_{1112} - C_{2222})\eta_{AC}^3 + \frac{1}{24}C_{12222}\eta_{AC}^4, \tag{12}$$

$$\Sigma_2^{arm} = C_{11}\eta_{AC} + \frac{1}{2}C_{222}\eta_{AC}^2 + \frac{1}{6}C_{2222}\eta_{AC}^3 + \frac{1}{24}C_{22222}\eta_{AC}^4. \tag{13}$$

For EQ tension ($\eta_{AC} = \eta_{ZZ} = \eta_{EQ} > 0$), the strain tensor is

$$\eta_{ij}^{EQ} = \begin{pmatrix} \eta_{EQ} & 0 \\ 0 & \eta_{EQ} \end{pmatrix}, \tag{14}$$

The corresponding deformation gradient tensor $\boldsymbol{F}_{EQ}$ for EQ tension is

$$\boldsymbol{F}_{EQ} = \begin{pmatrix} \varepsilon_{EQ} + 1 & 0 \\ 0 & \varepsilon_{EQ} + 1 \end{pmatrix}, \tag{15}$$

where ε_{EQ} is the nominal strain under EQ tension. The 2nd P–K stress versus Lagrangian strain relationship for EQ tension is

$$\begin{aligned} \Sigma_1^{EQ} = \Sigma_2^{EQ} &= (C_{11} + C_{12})\eta_{EQ} + \frac{1}{2}(2C_{111} - C_{222} + 3C_{112})\eta^2 \\ &+ \frac{1}{6}\left(\frac{3}{2}C_{1111} + 4C_{1112} - \frac{1}{2}C_{2222} + 3C_{1122}\right)\eta^3 \\ &+ \frac{1}{24}(3C_{11111} + 10C_{11112} - 5C_{12222} + 10C_{11122} - 2C_{22222})\eta^4. \end{aligned} \tag{16}$$

From the definition of Lagrangian strain $\boldsymbol{\eta}$, we can obtain

$$\boldsymbol{\eta} = \boldsymbol{\varepsilon} + \frac{1}{2}\boldsymbol{\varepsilon}^2, \tag{17}$$

where $\boldsymbol{\varepsilon}$ represents the nominal strain ε_{AC}, ε_{ZZ}, and ε_{EQ}, respectively.

3.4. Elastic constants

Fig. 5 shows five relationships of the 2nd Piola–Kirchhoff (P–K) stress versus Lagrangian strain under three types of tensions obtained from the DFT calculations. All fourteen elastic constants appear in the stress–strain relationships for the three special cases collectively (Eqs. (8), (9), (12), (13), and (16)). The values of the elastic constants can be determined by fitting these equations to the DFT results as illustrated in Fig. 5. The dependent nonzero components of SOEC, TOEC, FOEC, and FFOEC are summarized in Table 1. Note that the components of the TOEC and FFOEC tensors are all negative, which ensures that the elastic stiffness softens with strain up to ultimate strain. The in-plane Young modulus E and Poisson's ratio ν can be obtained from the following relationships: $E = (C_{11}^2 - C_{12}^2)/C_{11}$ and $\nu = C_{12}/C_{11}$. We have $E = 334.77$ N/m, $\nu = 0.18$ N/m for monolayer GaSe at small tension.

Table 1
Nonzero independent components for the SOEC, TOEC, FOEC, and FFOEC tensor components.

SOEC (N/m)	TOEC (N/m)	FOEC (N/m)	FFOEC (N/m)
$C_{11} = 93.4$	$C_{111} = -707.3$	$C_{1111} = 4323.1$	$C_{11111} = -14492.6$
$C_{12} = 23.7$	$C_{112} = -61.8$	$C_{1112} = 275.3$	$C_{11112} = -1301.9$
	$C_{222} = -534.8$	$C_{1122} = 1333.7$	$C_{11122} = -3216.8$
		$C_{2222} = 1247.4$	$C_{12222} = -5189.5$
			$C_{22222} = -2474.9$

Under large hydrostatic pressure, it is useful to describe the nonlinear elastic properties of materials by the pressure dependent elastic constants $\widetilde{C}_{ij}$. For most applications, it is sufficient to only consider the linear terms in the external hydrostatic pressure. When pressure is applied, the pressure dependent second-order elastic constants $(\widetilde{C}_{11}, \widetilde{C}_{22}, \widetilde{C}_{12})$ and corresponding derivatives with pressure $(\widetilde{C}'_{11}, \widetilde{C}'_{22}, \widetilde{C}'_{12})$ can be obtained from C_{11}, C_{22}, C_{12}, C_{111}, C_{112}, C_{222}, E, and v as:

$$\widetilde{C}_{11} = C_{11} - (C_{111} + C_{112})\frac{1-v}{E}P, \tag{18}$$

$$\widetilde{C}'_{11} = -(C_{111} + C_{112})\frac{1-v}{E}, \tag{19}$$

$$\widetilde{C}_{22} = C_{11} - C_{222}\frac{1-v}{E}P, \tag{20}$$

$$\widetilde{C}'_{22} = -C_{222}\frac{1-v}{E}, \tag{21}$$

$$\widetilde{C}_{12} = C_{12} - C_{112}\frac{1-v}{E}P, \tag{22}$$

$$\widetilde{C}'_{12} = -C_{112}\frac{1-v}{E}. \tag{23}$$

Calculated $\widetilde{C}'_{11}, \widetilde{C}'_{22}, \widetilde{C}'_{12}$ are 6.52, 4.53, and 0.52, respective. $\widetilde{C}'_{ij}$ can be measured by the experiments. It is very interesting to compare our results with the experimental values, but there has been no relevant report so far.

4. Conclusion

In summary, we have studied the mechanical stabilities and nonlinear elastic properties of monolayer GaSe under tension based on first-principles DFT calculations. The ultimate strengths of monolayer GaSe under armchair, zigzag, and equiaxial tensions are 8.624 N/m, 10.466 N/m, and 8.838 N/m, respectively. Corresponding ultimate strains are 0.244, 0.473, and 0.275, respectively. For the equiaxial tension, monolayer GaSe becomes mechanically instable and the plastic deformation occurs beyond the ultimate strain.

The total fourteen nonzero independent nonlinear elastic constants of monolayer GaSe have been obtained by combining continuum elasticity theory and the homogeneous deformation method. Nonlinear behavior initiates at about 0.01 strain observing the strain energy density and stress versus strain relationships. We have also obtained Young's modulus (E = 334.77 N/m) and Poisson'sratio (v = 0.18 N/m) for monolayer GaSe at small tension. Calculated the pressure derivatives of second-order elastic moduli $\widetilde{C}'_{11}, \widetilde{C}'_{22},$ and $\widetilde{C}'_{12}$ are 6.62, 4.68, and 0.54, respective.

Calculated values of ultimate stresses and strains, and the in-plain Young's modulus are all positive. It indicates that monolayer GaSe is mechanically stable. Our work can contribute to understand the mechanical properties of monolayer GaSe and calculated data can be applied to finite element analyses models for its applications at large scale.

Acknowledgement

This work was supported by the National Natural Science Foundation of China (Grant Nos. 11304192, 21373156), Scientific Research Program Funded by Shaanxi Provincial Education Department, China (Grant No. 12JK0972), and the Open Program of State Key Laboratory of Functional Materials for Informatics.

References

[1] C. Lee, X. Wei, J.W. Kysar, J. Hone, Measurement of the elastic properties and intrinsic strength of monolayer graphene, Science 321 (2008) 385–388.
[2] K.S. Novoselov, Technology: rapid progress in producing graphene, Nature 505 (2014). 291–291.
[3] S.Z. Butler, S.M. Hollen, L. Cao, Y. Cui, et al, Progress challenges, and opportunities in two-dimensional materials beyond graphene, Acs Nano 7 (2013) 2898–2926.

[4] K.S. Novoselov, V.I. Falko, L. Colombo, P.R. Gellert, M.G. Schwab, K. Kim, A roadmap for graphene, Nature 490 (2012) 192–200.
[5] L. Song, L. Ci, H. Lu, P.B. Sorokin, C. Jin, J. Ni, A.G. Kvashnin, D.G. Kvashnin, J. Lou, B.I. Yakobson, P.M. Ajayan, Large scale growth and characterization of atomic hexagonal boron nitride layers, Nano Lett. 10 (2010) 3209–3215.
[6] J.N. Coleman, M. Lotya, A. O'Neill, S.D. Bergin, et al, Two-dimensional nanosheets produced by liquid exfoliation of layered materials, Science 331 (2011) 568–571.
[7] B. Radisavljevic, A. Radenovic, J. Brivio, V. Giacometti, A. Kis, Single-layer MoS2 transistors, Nat. Nano 6 (2011) 147–150.
[8] Y.-H. Lee, X.-Q. Zhang, W. Zhang, M.-T. Chang, et al, Synthesis of large-area MoS2 atomic layers with chemical vapor deposition, Adv. Mater. 24 (2012) 2320–2325.
[9] A.M. van der Zande, P.Y. Huang, D.A. Chenet, et al, Grains and grain boundaries in highly crystalline monolayer molybdenum disulphide, Nat. Mater. 12 (2013) 554–561.
[10] S. Najmaei, Z. Liu, W. Zhou, X. Zou, G. Shi, S. Lei, B.I. Yakobson, J.-C. Idrobo, P.M. Ajayan, J. Lou, Vapour phase growth and grain boundary structure of molybdenum disulphide atomic layers, Nat. Mater. 12 (2013) 754–759.
[11] R.C. Cooper, C. Lee, C.A. Marianetti, X. Wei, J. Hone, J.W. Kysar, Nonlinear elastic behavior of two-dimensional molybdenum disulfide, Phys. Rev. B 87 (2013) 035423.
[12] Y.-H. Lee, L. Yu, H. Wang, W. Fang, X. Ling, Y. Shi, C.-T. Lin, J.-K. Huang, M.-T. Chang, C.-S. Chang, M. Dresselhaus, T. Palacios, L.-J. Li, J. Kong, Synthesis and transfer of single-layer transition metal disulfides on diverse surfaces, Nano Lett. 13 (2013) 1852–1857.
[13] Y. Zhang, Y. Zhang, Q. Ji, J. Ju, H. Yuan, J. Shi, T. Gao, D. Ma, M. Liu, Y. Chen, X. Song, H.Y. Hwang, Y. Cui, Z. Liu, Controlled growth of high-quality monolayer WS2 layers on sapphire and imaging its grain boundary, ACS Nano 7 (2013) 8963–8971.
[14] A.M. Jones, H. Yu, N.J. Ghimire, S. Wu, G. Aivazian, J.S. Ross, B. Zhao, J. Yan, D.G. Mandrus, D. Xiao, W. Yao, X. Xu, Optical generation of excitonic valley coherence in monolayer WSe2, Nat. Nano 8 (2013) 634–638.
[15] H. Fang, S. Chuang, T.C. Chang, K. Takei, T. Takahashi, A. Javey, High-performance single layered WSe2 p-FETs with chemically doped contacts, Nano Lett. 12 (2012) 3788–3792.
[16] S. Lei, L. Ge, Z. Liu, S. Najmaei, G. Shi, G. You, J. Lou, R. Vajtai, P.M. Ajayan, Synthesis and photoresponse of large GaSe atomic layers, Nano Lett. 13 (2013) 2777–2781.
[17] X.F. Li, M.W. Lin, A.A. Puretzky, et al, Controlled vapor phase growth of single crystalline, two-dimensional GaSe crystals with high photoresponse, Sci. Rep.-UK 4 (2014).
[18] P. Hu, Z. Wen, L. Wang, P. Tan, K. Xiao, Synthesis of few-layer GaSe nanosheets for high performance photodetectors, ACS Nano 6 (2012) 5988–5994.
[19] D.J. Late, B. Liu, J. Luo, A. Yan, H.S.S.R. Matte, M. Grayson, C.N.R. Rao, V.P. Dravid, GaS and GaSe ultrathin layer transistors, Adv. Mater. 24 (2012) 3549–3554.
[20] P. Hu, L. Wang, M. Yoon, J. Zhang, W. Feng, X. Wang, Z. Wen, J.C. Idrobo, Y. Miyamoto, D.B. Geohegan, K. Xiao, Highly responsive ultrathin GaS nanosheet photodetectors on rigid and flexible substrates, Nano Lett. 13 (2013) 1649–1654.
[21] G.W. Mudd, S.A. Svatek, T. Ren, A. Patanè, et al, Tuning the bandgap of exfoliated inse nanosheets by quantum confinement, Adv. Mater. 25 (2013) 5714–5718.
[22] M. Genut, L. Margulis, G. Hodes, R. Tenne, Preparation and microstructure WS2 thin films, Thin Solid Films 217 (1992) 91–97.
[23] A. Kuhn, A. Chevy, R. Chevalier, Refinement of the 2H GaS [beta]-type, Acta Crystallogr. Sec. B 32 (1976) 983–984.
[24] D.J. Late, B. Liu, H.S.S.R. Matte, C.N.R. Rao, V.P. Dravid, Rapid characterization of ultrathin layers of chalcogenides on SiO_2/Si substrates, Adv. Funct. Mater. 22 (2012) 1894–1905.
[25] C.-H. Ho, M.-H. Hsieh, C.-C. Wu, Photoconductance and photoresponse of layer compound photodetectors in the UV–visible region, Rev. Sci. Instrum. 77 (2006).
[26] G. Shen, D. Chen, P.-C. Chen, C. Zhou, Vapor–solid growth of one-dimensional layer-structured gallium sulfide nanostructures, ACS Nano 3 (2009) 1115–1120.
[27] X. Wei, B. Fragneaud, C.A. Marianetti, J.W. Kysar, Nonlinear elastic behavior of graphene: ab initio calculations to continuum description, Phys. Rev. B 80 (2009) 205407.
[28] Q. Peng, C. Liang, W. Ji, S. De, A theoretical analysis of the effect of the hydrogenation of graphene to graphane on its mechanical properties, Phys. Chem. Chem. Phys. 15 (2013) 2003–2011.
[29] Q. Peng, X. Wen, S. De, Mechanical stabilities of silicene, RSC Adv. 3 (2013) 13772–13781.
[30] G. Kresse, J. Hafner, Ab initio molecular dynamics for open-shell transition metals, Phys. Rev. B 48 (1993) 13115–13118.
[31] G. Kresse, J. Furthmüller, Efficiency of ab-initio total energy calculations for metals and semiconductors using a plane-wave basis set, Comput. Mater. Sci. 6 (1996) 15–50.
[32] D.M. Ceperley, B.J. Alder, Ground state of the electron gas by a stochastic method, Phys. Rev. Lett. 45 (1980) 566–569.
[33] J. Zhou, R. Huang, Internal lattice relaxation of single-layer graphene under in-plane deformation, J. Mech. Phys. Solids 56 (2008) 1609–1623.
[34] R.A. Toupin, B. Bernstein, Sound waves in deformed perfectly elastic materials. Acoustoelastic effect, J. Acoust. Soc. Am. 33 (1961) 216–225.
[35] J.F. Nye, Physical Properties of Crystals, Oxford Science Publications, Oxford, 1985.